Analysis of Arbitrarily Oriented Microstrip Lines Utilizing a Quasi-Dynamic Approach

Tawfik Rahal Arabi, *Member, IEEE*, Arthur T. Murphy, *Fellow, IEEE*, Tapan K. Sarkar, *Senior Member, IEEE*, Roger F. Harrington, *Fellow, IEEE*, and Antonije R. Djordjević

***Abstract*—In this paper a "quasi-dynamic" approach is presented for the analysis of arbitrarily oriented printed microstrip circuits. The metallic structures are assumed to be planar metals of zero thickness. The quasi-dynamic approach differs from the quasi-static solution in the sense that phase variation is included in the quasi-dynamic analysis. The region of validity of the quasi-dynamic approach is investigated. Finally, numerical results are presented to illustrate the use of this technique.**

I. Introduction

In this presentation, the Green's function approach for the analysis of electromagnetic scattering from printed circuits lying at the air–dielectric interface is utilized. The dielectric is backed by a ground plane. For the dynamic approach, the Green's functions are quite complicated and require the evaluation of certain semi-infinite integrals. This paper describes the derivation of a "quasi-dynamic" approach. For this approach certain approximations have been made in the evaluation of the semi-infinite integrals, resulting in much simpler expressions. Regions of validity of the quasi-dynamic approach are also outlined. Finally, examples are presented.

II. Horizontal Dipoles over a Dielectric

An elementary horizontal electric dipole of moment Idx and oriented in the x direction is located at a height $z=0$ above a dielectric interface. The dielectric is backed by a ground plane at $z=-h$. In this case two components of the Hertzian vector, π_x and π_z, of the electric type are necessary to specify the fields completely. Assuming a time variation $\exp(j\omega t)$, the Hertz potentials satisfy the following wave equation [1]:

$$(\nabla^2+k_2^2)\vec{\pi}_1=\vec{e}_x\frac{Idx}{j\omega\epsilon}\partial(x-x')\partial(y-y')\partial(z-z') \quad (1)$$

$$(\nabla^2+k_2^2)\vec{\pi}_2=0 \quad (2)$$

Manuscript received October 31, 1989; revised July 24, 1990. This work was supported by E. I. Du Pont De Nemours and Co., Wilmington, DE, by the Army Research Office, Research Triangle Park NC (Contract DAAL03-88-K-0133), by the Cornell National Science Foundation Super Computing Facilty, and by the Northeast Parallel Architectures Center at Syracuse University.

T. Rahal Arabi is with the Department of Electrical Engineering, Syracuse University, Syracuse, NY 13244, and with the Experimental Station, DuPont Electronics, Wilmington, DE 19880.

A. T. Murphy is with the Experimental Station, DuPont Electronics, Wilmington, DE 19880.

T. K. Sarkar and R. F. Harrington are with the Department of Electrical Engineering, Syracuse University, Syracuse, NY 13244.

A. R. Djordjević is with the University of Belgrade, Belgrade, Yugoslavia.

IEEE Log number 9040570.

where

$$k_1=\omega^2\mu\epsilon_1 \quad \text{and} \quad k_2=\omega^2\mu\epsilon_2.$$

The electric and magnetic field vectors are derived from the Hertzian vector:

$$\vec{E}=k^2\vec{\pi}+\nabla(\nabla\cdot\vec{\pi})=-j\omega\vec{A}-\nabla\phi \quad (3)$$

$$\vec{H}=j\omega\epsilon(\nabla\times\vec{\pi})=\nabla\times\vec{A} \quad (4)$$

respectively. Therefore the Hertzian vectors are related to the conventional magnetic vector potential A and the scalar potential ϕ by

$$\vec{A}=j\omega\mu\epsilon\vec{\pi} \quad (5)$$

$$\phi=\nabla\cdot\vec{\pi}. \quad (6)$$

The complete solution for the Hertzian vectors has been presented in [1] and [2] and is given by

$$A_{x1}=\frac{\mu_0 Idx}{4\pi}\int_c\frac{H_0^{(2)}(\lambda\rho)\lambda e^{-u_0 z}}{\text{DTE}}d\lambda \quad (7)$$

$$A_{x2}=\frac{\mu_0 Idx}{4\pi}\int_c\frac{H_0^{(2)}(\lambda\rho)\lambda\sinh[u(z+h)]}{\text{DTE}\sinh(uh)}d\lambda \quad (8)$$

$$A_{z1}=\frac{\mu_0 Idx(\epsilon_r-1)}{4\pi}\frac{\partial}{\partial x}\int_c\frac{H_0^{(2)}(\lambda\rho)\lambda e^{-u_0 z}}{\text{DTE DTM}}d\lambda \quad (9)$$

$$A_{z2}=\frac{\mu_0 Idx(\epsilon_r-1)}{4\pi}\frac{\partial}{\partial x}\int_c\frac{H_0^{(2)}(\lambda\rho)\lambda\cosh[u(z+h)]}{\text{DTE DTM}\cosh(uh)}d\lambda \quad (10)$$

where

$$u_0=jk_{z0}=\sqrt{\lambda^2-k_0^2} \quad (11)$$

$$u=jk_{z2}=\sqrt{\lambda^2-\epsilon_r k_0^2} \quad (12)$$

$$\rho=\sqrt{(x-x')^2+(y-y')^2} \quad (13)$$

$$\text{DTE}=u_0+u\coth(uh) \quad (14)$$

$$\text{DTM}=\epsilon_r u_0+u\tanh(uh) \quad (15)$$

$$k_{z1,2}^2+\lambda^2=k_{1,2}^2 \quad (16)$$

and c represent integration from $-\infty$ to $+\infty$. Thus the zeros of DTE and DTM give the phase constants of the characteristic TE and TM modes propagating in such a structure. It is shown in [2] that for frequencies f such that $f<f_c=c/(4h\sqrt{\epsilon_r-1})$, where c is the velocity of light in free space, DTE has no real zeros, while DTM has only one real zero.

The frequency f_c which can be considered the cutoff frequency of the first TE mode, is usually very high for usual microstrip substrates. For instance for $\epsilon_r = 10$ and $h = 1$ mm, we find $f_c = 25$ GHz. Hence we always assume $f < f_c$ and therefore DTE has no real zeros while DTM always has a real zero in the interval $k_0 < \lambda < \sqrt{\epsilon_r} k_0$.

III. Formulation of the Problem

It is assumed that the printed circuits are of zero thickness and that the widths of the strips are quite small compared with the wavelength so that the variation of the current along the transverse direction does not change significantly along the length of the printed circuit. The current distribution across the transverse section then depends on the ratio w/h, where w is the strip width and h is the thickness of the substrate. It is commonly assumed that the current has a square root behavior across the transverse section, i.e., [3], [4],

$$Q(y) = \frac{1}{\pi\sqrt{\left(\frac{w}{2}\right)^2 - y^2}}, \qquad \frac{-w}{2} \leqslant y \leqslant \frac{w}{2} \tag{17}$$

so that the current has a singularity at $y = \pm w/2$. This distribution is correct, however, if $w/h \ll 1$. If $w/h \gg 1$, then a better choice for the transverse variation of the current is a constant distribution [4], [5], given by

$$Q(y) = \frac{1}{w}, \qquad \frac{-w}{2} \leqslant y \leqslant \frac{w}{2}. \tag{18}$$

Thus the printed circuits are modeled here by strips where the transverse component of the current distribution is assumed to be known and one is then solving for the longitudinal distribution.

A. Moment Method Formulation

The problem of finding the current distribution on arbitrarily oriented zero-thickness metallic strip elements is but a particular case of the general boundary value problem involving conducting bodies in a known impressed field, $\vec{E}^i$. The boundary condition at the surface of each perfect conductor is that the tangential component of the electric field must be zero. Since we are approximating the circuits by thin strips, the following approximations can be made:

a) The currents are assumed to flow only in the axial direction, with a transverse variation that is assumed to be known.
b) The boundary condition ($\vec{E}_{\tan}^{\text{total}} = \vec{0}$) is applied to the axial component of $\vec{E}^{\text{total}}$ on each strip surface.

By utilizing these approximations we compute the current density on the strips as $\vec{E}^i_{\text{total}} + \vec{E}^s_{\text{total}} = \vec{0}$ on the surface of the strip, or

$$\vec{E}^i_{\tan} = -\vec{E}^s_{\tan} = \left(j\omega\vec{A} + \nabla\phi\right) = L\left(\vec{J}_s\right) \tag{19}$$

where $L(\vec{J}_s)$ defines the integro-differential operator on the surface current density $\vec{J}_s$ and the subscript "tan" refers to the tangential component. Then $L(\vec{J}_s) = \vec{E}^i_{\tan}$ on the surface of the strip and $\vec{I} = \vec{0}$ at the ends of the strip.

By applying the method of moments, we can reduce the functional equation to a matrix equation. This matrix equation is obtained by first expanding the unknown current distribution J_s in terms of triangular expansion functions T_n for the longitudinal variation of the current with unknown coefficients a_n. Therefore

$$J_s = \sum_i^N a_i Q_i(y) T_i(x) \tag{20}$$

where $Q(y_i)$ denotes the transverse distribution of the current, which is assumed to be known. By substituting J_s in the operator equation and weighting the residuals by the functions $Q_j(y)T_j(x)$, we obtain

$$\langle R_i; T_j\rangle = a_i\langle Q_i(y)L(T_i); Q_j(y)T_j\rangle = \langle E^i_{\tan}; Q_j(y)T_j\rangle \tag{21}$$

where $\langle , \rangle$ denotes the usual Hilbert inner product. Therefore the matrix equation can be written as

$$[Z]\vec{A} = \vec{V} \tag{22}$$

where $[Z]$ is the generalized impedance matrix of dimension $N \times N$ whose ij element is given by

$$Z_{ij} = \langle L(Q_i(y)T_i(x)), Q_j(y)T_j(x)\rangle. \tag{23}$$

$\vec{A}$ is a column vector containing the unknown coefficients a_n while $\vec{V}$ is the generalized voltage matrix, given by

$$V_j = \langle \vec{E}^i_{\tan}; Q_j(y)T_j(x)\rangle. \tag{24}$$

The desired solution for $[A]$ is obtained by inverting $[Z]$ as

$$\vec{A} = [Z]^{-1}\vec{V}. \tag{25}$$

When an impressed voltage is applied at a point, then only that E^i remains nonzero and all other entries in $\vec{V}$ are zeros.

B. Computation of the Mutual Impedance Between Two Arbitrarily Oriented Current Elements

We next compute the mutual impedance between two arbitrarily oriented current elements l_i and l_j carrying current distributions $Q_i(y)T_i(x)$ and $Q_j(y)T_j(x)$, respectively, and situated over the interface. In order to proceed, we reorient the coordinate system and choose the direction of the $\vec{x}$ axis as the direction of T_i. The tangential electric field, $\vec{E}_{\tan}$, at the interface between the air and the dielectric medium ($z = 0$) due to an HED is given by

$$\vec{E}_{\tan} = -j\omega A_x\vec{e}_x + \frac{1}{j\omega\mu\epsilon}\nabla(\nabla\cdot\vec{A}) \tag{26}$$

which can be conveniently written as

$$\vec{E}_{\tan} = C_1 G_x\vec{e}_x + C_2\nabla\left(\frac{\partial}{\partial x}G_v\right) \tag{27}$$

where

$$C_1 = \frac{-j\omega\mu_0 I dx}{4\pi} \qquad C_2 = \frac{I dx}{4\pi j\omega\mu\epsilon} \tag{28}$$

$$G_x = \int_C \frac{H_0^{(2)}(\lambda\rho)\lambda}{\text{DTE}}\,d\lambda \tag{29}$$

$$G_v = \int_C \frac{H_0^{(2)}(\lambda\rho)\lambda N}{\text{DTE DTM}}, \qquad N = u_0 + u\tanh(uh). \tag{30}$$

Thus, the tangential field due to current element $Q_i(y)T_i(x)$

locally oriented in the x direction is given by

$$\vec{E}_{\tan} = C_1\vec{e}_x\int_{w_i} Q_i(y')\,dy'\int_{l_i} G_x(x,y,x',y')T_i(x')\,dx' + C_2\nabla\left\{\int_{w_i} Q_i(y')\,dy'\int_{l_i}\frac{\partial}{\partial x}G_v(x,y,x',y')T_i(x')\,dx'\right\}. \quad (31)$$

The interaction Z_{ij} between a locally $\vec{x}$-directed current element, $Q_i(y)T_i(x)\vec{e}_x$, and a current element $Q_j(y)T_j(x)\vec{e}_j$ oriented in an arbitrary direction $\vec{e}_j$ is therefore given by

$$Z_{ij} = C_1\int_{w_j} Q_j(y)\,dy\int_{l_j} T_j(x)\,dx\,\vec{e}_j\cdot\vec{e}_x\int_{w_i} Q_i(y')\,dy' \cdot\int_{l_i} G_x(x,y,x',y')T_i(x')\,dx' + C_2\int_{w_j} Q_j(y)\,dy\int_{l_j} T_j(x)\,dx(\vec{e}_j\cdot\nabla) \cdot\int_{w_i} Q_i(y')\,dy'\int_{l_i} T_i(x')\frac{\partial}{\partial x}G_v(x,y,x',y')\,dx'. \quad (32)$$

Noting that

$$\frac{\partial}{\partial x}G_v = -\frac{\partial}{\partial x'}G_v \quad\text{and}\quad \vec{e}_j\cdot\nabla G = \frac{\partial}{\partial x_j}G$$

$T_i(x)$ and $T_j(x)$ are identically zero at the element ends, and using integration by parts, the derivative and the gradient operator acting on G_v can be transformed to derivatives on the current elements. Equation (31) thus reduces to

$$Z_{ij} = \int_{w_j} Q_j(y)\,dy\int_{w_i} Q_i(y')\,dy'\left\{C_1\int_{l_j} dx\int_{l_i} T_j(\vec{x})\cdot T_i(\vec{x}')\,dx' + C_2\int_{l_j}\frac{\partial}{\partial x}T_j(x)\,dx\int_{l_i}\frac{\partial}{\partial x'}T_i(x')G_v(x,y,x',y').\right. \quad (33)$$

The derivatives of the triangular functions can be easily calculated analytically and they form the bipolar pulse functions. So the computation of the mutual impedance between two arbitrarily oriented triangular pulse functions situated over a dielectric interface is equivalent to evaluating the integrals of G_x and G_v. This is dealt with in the next section.

IV. Numerical Evaluation of G_x and G_v

In this paper two methods are utilized to evaluate the Green's functions G_x and G_v. The first is a dynamic solution in which the integrals are essentially evaluated in an exact manner; the second method deals with an approximate solution, where it is assumed that the width is small enough compared with the wavelength inside the dielectric that a "quasi-dynamic" approximation can be made. The two solutions are then compared in order to find the region of validity of the quasi-dynamic approximation.

A. Numerical Integration of the Infinite Integrals

The Green's functions G_x and G_v can be written (at the interface) as

$$G_x = \int_C \frac{H_0^{(2)}(\lambda\rho)\lambda}{\text{DTE}}\,d\lambda = 2\int_0^\infty J_0(\lambda\rho)\frac{\lambda}{\text{DTE}}\,d\lambda \quad (34)$$

$$G_v = \int_C \frac{H_0^{(2)}(\lambda\rho)\lambda N}{\text{DTE DTM}} = 2\int_0^\infty J_0(\lambda\rho)\left[\frac{\lambda N}{\text{DTE DTM}}\right]d\lambda. \quad (35)$$

We then subtract the asymptotic values of the integrals, so that we numerically have to evaluate smoother functions. We define

$$\begin{aligned} g_x &= G_x - \int_0^\infty J_0(\lambda\rho)\,d\lambda \\ &= G_x - \frac{1}{\rho} = 2\int_0^\infty J_0(\lambda\rho)\left[\frac{\lambda}{\text{DTE}} - 0.5\right]d\lambda \\ g_v &= G_v - \frac{2}{(\epsilon_r-1)}\int_0^\infty J_0(\lambda\rho)\,d\lambda = G_v - \frac{2}{\rho(\epsilon_r-1)} \\ &= \int_0^\infty J_0(\lambda\rho)\left[\frac{\lambda N}{\text{DTE DTM}} - \frac{1}{(\epsilon_r-1)}\right]d\lambda. \end{aligned} \quad (36)$$

The rationale for doing this is that as $\lambda\to\infty$, g_x and g_v approach zero at a faster rate than G_x and G_v. For the sake of simplicity we will also consider that the frequency of operation satisfies $f < c/(4h\sqrt{\epsilon_r - 1})$. Therefore DTE has no poles on the λ axis $[0,\infty]$ and the integral for g_x is well behaved. The other integral has one pole on the real axis $[k_0, \sqrt{\epsilon_r}k_0]$. The integrals of g_x and g_v are then evaluated in the same way as described in [2].

B. The Quasi-Dynamic Solution

In this approach we perform near-field approximations for the two integrals. The assumption $k_0\rho \ll 1$ leads to [2]

$$G_x = \frac{\exp(-jk_0r_0)}{r_0} - \frac{\exp(-jk_0r_1)}{r_1} \quad (37)$$

$$G_v = (1-\eta)\left\{\left[\frac{\exp(-jk_0r_0)}{r_0} - (1+\eta)\sum_{i=1}^{\infty}(-\eta)^{(i-1)}\frac{\exp(-jk_0r_i)}{r_i}\right.\right\} \quad (38)$$

where

$$r_i = \sqrt{\rho^2 + (2ih)^2} \quad\text{and}\quad \eta = \frac{\epsilon_r - 1}{\epsilon_r + 1}.$$

V. Region of Validity of the Quasi-Dynamic Solution

In order to find the region of validity of the quasi-dynamic solution, we compute the ratio of the Green's functions computed using the dynamic solution to those computed using the quasi-dynamic solution. Fig. 1 shows a plot of the ratio (R_{xm}) of the magnitude of G_x computed using the dynamic solution to that computed using the quasi-dynamic solution versus the normalized wavelength λ_0. The ratio is plotted for an ϵ_r of 2 and different values of h. Similarly,

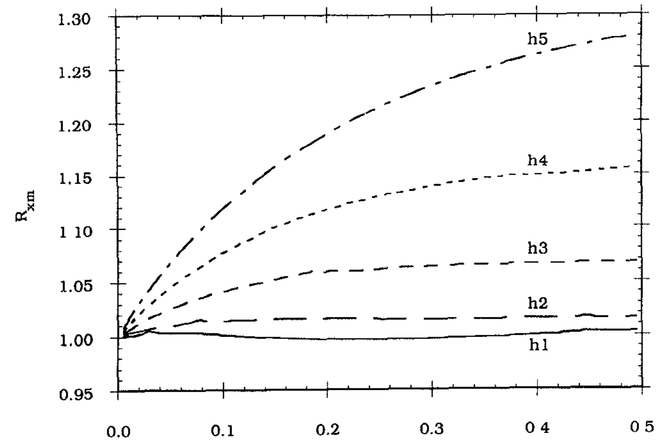

Fig. 1. The ratio R_{xm} of the magnitude of the Green's function G_x computed using the dynamic approach to the magnitude of the Green's function computed using the quasi-dynamic approach versus the normalized distance in terms of the free-space wavelength λ_0 for different values of h: $\epsilon_r = 2.0$, $h1 = 0.01$, $h2 = 0.025$, $h3 = 0.05$, $h4 = 0.075$, and $h5 = 0.1$.

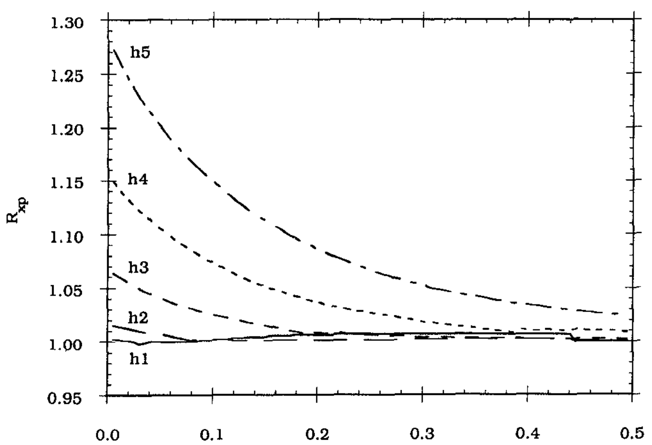

Fig. 2. The ratio R_{xm} of the phase of the Green's function G_x computed using the dynamic approach to the phase of the Green's function G_x computed using the quasi-dynamic approach versus the normalized distance in terms of the free-space wavelength λ_0 for different values of h: $\epsilon_r = 2.0$, $h1 = 0.01$, $h2 = 0.025$, $h3 = 0.05$, $h4 = 0.075$, and $h5 = 0.1$.

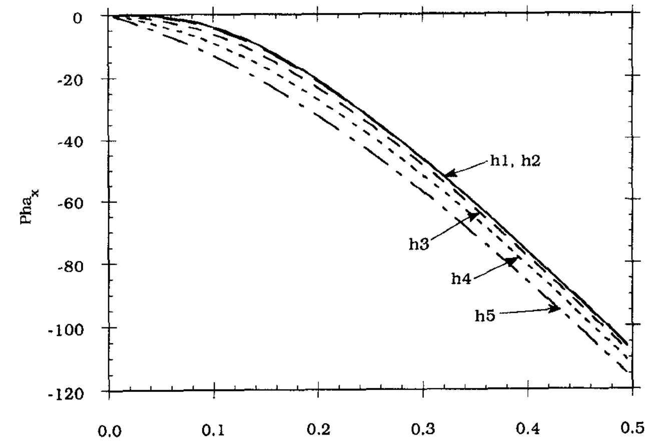

Fig. 3. The phase pha_x of the Green's function G_x computed using the dynamic approach versus the normalized distance in terms of the free-space wavelength λ_0 for different values of h: $\epsilon_r = 2.0$, $h1 = 0.01$, $h2 = 0.025$, $h3 = 0.05$, $h4 = 0.075$, and $h5 = 0.1$.

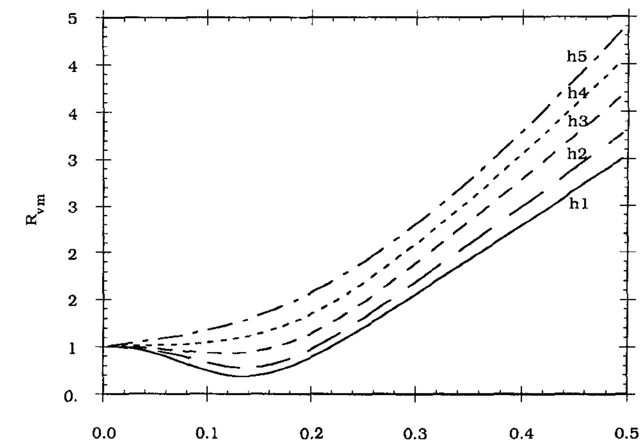

Fig. 4. The ratio R_{tm} of the magnitude of the Green's function G_t computed using the dynamic approach to the magnitude of the Green's function G_t computed using the quasi-dynamic approach versus the normalized distance in terms of the free-space wavelength λ_0 for different values of h: $\epsilon_r = 2.0$, $h1 = 0.01$, $h2 = 0.025$, $h3 = 0.05$, $h4 = 0.075$, and $h5 = 0.1$.

Fig. 2 shows the ratio (R_{xp}) of the phase of G_x computed using the dynamic solution to that computed using the quasi-dynamic solution. For values of h up to $0.075\lambda_0$, the value of G_x (magnitude and phase) predicted by the quasi-dynamic solution is always within 15% of the value predicted by the dynamic solution for all values of ρ. Furthermore it is clear from Figs. 1 and 2 that the error in the magnitude of G_x tends to a constant that depends on ϵ_r and h only, while the error in the phase goes to zero in the far-field region. This is expected since the quasi-dynamic solution behaves as $1/\rho^2$ in the far-field region at the interface.

Fig. 3 shows the phase of G_x in degrees as a function of the normalized distance in terms of λ_0. It can be seen that the phase is not negligible for all values of the normalized distance ρ. Thus while the value of G_x predicted by quasi-static solution is valid only in the region of zero phase, that is, in the region very close to the source, the value predicted by the quasi-dynamic solution remains valid for all values of ρ and therefore is more accurate.

Fig. 4 shows the ratio (R_{tm}) of the magnitude of G_v computed using the dynamic solution to that computed using the quasi-dynamic solution versus the normalized distance. This ratio has a peculiar behavior; it has a dip at about $0.12\lambda_0$ that is more pronounced for smaller values of h. Such behavior was also predicted by Mosig and Sarkar in [2]. The magnitude of G_v predicted by the quasi-dynamic solution remains valid for values of h up to $0.1\lambda_0$ and ρ less than $0.075\lambda_0$ while the phase is negligible in this region.

Next we fix the substrate height h and vary the dielectric constant ϵ_r. Thus Figs. 5 and 6 represent the same cases as Figs. 1 and 2 while Figs. 7 and 8 represent the same case as Fig. 4 except that the substrate height h is fixed at $0.025\lambda_0$ and ϵ_r is allowed to vary. It can be seen that while R_{xm} and R_{xp} have basically the same dependence on h and $\sqrt{\epsilon_r}$, R_{vm} has a much stronger dependence of ϵ_r than on h.

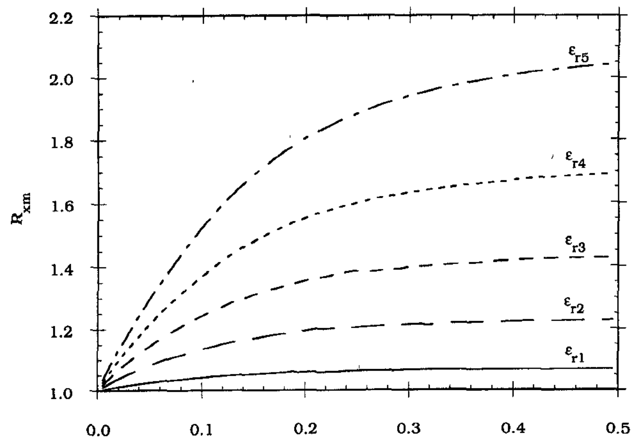

Fig. 5. The ratio R_{xm} of the magnitude of the Green's function G_x computed using the dynamic approach to the magnitude of the Green's function G_x computed using the quasi-dynamic approach versus the normalized distance in terms of the free-space wavelength λ_0 for different values of ϵ_r: $h = 0.025$, $\epsilon_{r1} = 2.0$, $\epsilon_{r2} = 4.0$, $\epsilon_{r3} = 6.0$, $\epsilon_{r4} = 8.0$, and $\epsilon_{r5} = 10.0$.

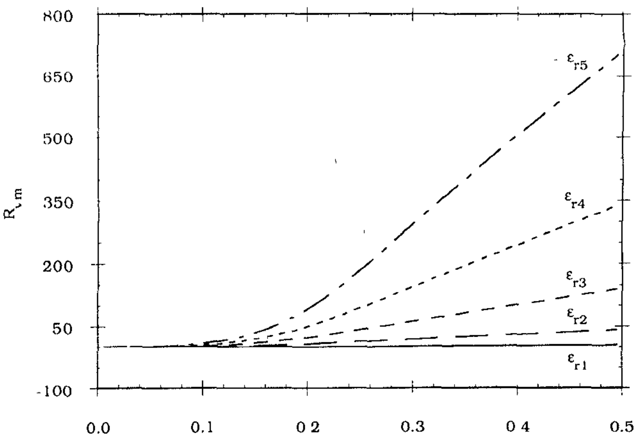

Fig. 7. The ratio R_{vm} of the magnitude of the Green's function G_v computed using the dynamic approach to the magnitude of the Green's function G_v computed using the quasi-dynamic approach versus the normalized distance in terms of the free-space wavelength λ_0 for different values of ϵ_r: $h = 0.025$, $\epsilon_r 1 = 2.0$, $\epsilon_{r2} = 4.0$, $\epsilon_{r3} = 6.0$, $\epsilon_{r4} = 8.0$, and $\epsilon_{r5} = 10.0$.

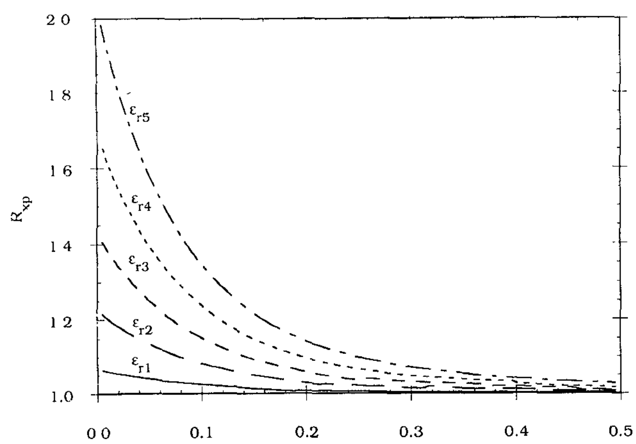

Fig. 6. The ratio R_{xp} of the phase of the Green's function G_x computed using the dynamic approach to the phase of the Green's function G_x computed using the quasi-dynamic approach versus the normalized distance in terms of the free-space wavelength λ_0 for different values of ϵ_r: $h = 0.025$, $\epsilon_{r1} = 2.0$, $\epsilon_{r2} = 4.0$, $\epsilon_{r3} = 6.0$, $\epsilon_{r4} = 8.0$, and $\epsilon_{r5} = 10.0$.

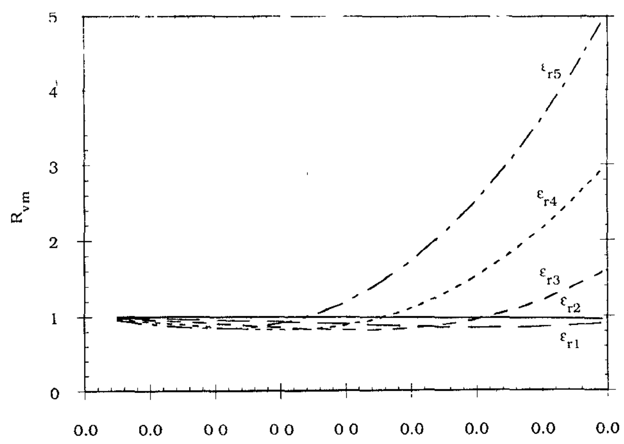

Fig. 8. A magnified scale of the ratio R_{vm} of the magnitude of the Green's function G_v computed using the dynamic approach to the magnitude of the Greens' function G_v computed using the quasi-dynamic approach versus the normalized distance in terms of the free-space wavelength λ_0 for different values of ϵ_r: $h = 0.025$, $\epsilon_{r1} = 2.0$, $\epsilon_{r2} = 4.0$, $\epsilon_{r3} = 6.0$, $\epsilon_{r4} = 8.0$, and $\epsilon_{r5} = 10.0$.

VI. Numerical Examples

Once G_x and G_v have been computed, the integrals appearing in the generalized impedance elements are then computed numerically using a Gaussian quadrature. To evaluate the S parameters of an N-port network, we excite one port at a time. The port is excited by having 1 V applied at a position quite far away from the input terminals of the network. We then solve the field problem utilizing triangular expansion functions for the current and find the current distribution on the entire structure. In order to have a circuit description we define the voltage at a point as the line integral of the vertical component of the electric field from $-h$ to 0. Equivalently, it is given by the second term in the expression (3) for the electric field, i.e.,

$$\vec{E} = -j\omega\vec{A} - \nabla V = -\nabla V$$

(under quasi-dynamic conditions).

The voltage at a point (x, y) arising from the current distributions on all the conducting strips can thus be written as

$$V(x,y) = \frac{1}{j4\pi\omega\epsilon_0} \sum_{p=1}^{N} \cdot \int_{W_p} dy_p\, Q_p(y_p) \int_{l_p} \frac{dJ_{sp}}{dx_p} G_v(x_p, y_p; x, y)\, dx_p \quad (39)$$

where W_p, l_p, and J_{sp} are the width, length, and current distribution of the pth strip, $\vec{x}_p$ denotes the direction of the current on the pth strip, and N is the total number of strips on the circuit.

In order to obtain the two-port network parameters, two reference planes are defined. For one particular excitation let V_1, I_1 and V_2, I_2 be the two voltages and currents at the two reference planes. We consider a second excitation to the port which was not previously excited. The voltages and currents at the same two reference planes previously defined are denoted by V_1', I_1' and V_2', I_2'. Then the $[A\ B\ C\ D]$

parameters of the network contained between the two preassigned reference planes are related by

$$\begin{bmatrix} A \\ B \\ C \\ D \end{bmatrix} = \begin{bmatrix} V_2 & I_2 & 0 & 0 \\ 0 & 0 & V_2 & I_2 \\ V_2' & I_2' & 0 & 0 \\ 0 & 0 & V_2' & I_2' \end{bmatrix} = \begin{bmatrix} V_1 \\ I_1 \\ V_1' \\ I_1' \end{bmatrix}. \tag{40}$$

From the $[A\ B\ C\ D]$ parameters, the S parameters or any other parameters of interest can be obtained.

A. Computation of the Characteristic Impedance

As a first example, consider a microstrip line of finite length $(1\lambda_0)$ of width $= 0.01\lambda_0$, $h = 0.01\lambda_0$, and $\epsilon_r = 10.0$. By defining the reference planes between two planes separated by $0.1\lambda_0$, we obtain the $[A\ B\ C\ D]$ matrix

$$\begin{bmatrix} A & C \\ B & D \end{bmatrix} = \begin{bmatrix} 0.4095 & -j45.80 \\ -j0.01819 & 0.4083 \end{bmatrix}.$$

From this 3-D analysis, we obtain such 2-D parameters as the characteristic impedance $Z_0^{3\mathrm{D}}$ and $\epsilon_{r\mathrm{eff}}$. By comparing the above matrix to the $[A\ B\ C\ D]$ matrix of a section of transmission line, we obtain $Z_0^{3\mathrm{D}} = 50.17$ and $\epsilon_{r\mathrm{eff}}^{3\mathrm{D}} = 6.46$.

From 2-D analysis [5] and from approximate analytical formulas [9] we obtain

$$Z_0^{2\mathrm{D}} = 49.15 \qquad \epsilon_{r\mathrm{eff}}^{2\mathrm{D}} = 6.65$$

and

$$Z_0^{a} = 48.33 \qquad \epsilon_{r\mathrm{eff}}^{a} = 6.85.$$

As a second example we consider $W = 0.05\lambda_0$, $h = 0.005\lambda_0$, and $\epsilon_r = 10.0$. We obtain the $[A\ B\ C\ D]$ matrix as

$$\begin{bmatrix} A & C \\ B & D \end{bmatrix} = \begin{bmatrix} 0.2310 & -j9.034 \\ -j0.1049 & 0.2304 \end{bmatrix}.$$

The 3-D results are thus given by $Z_0^{3\mathrm{D}} = 9.279$ and $\epsilon_{r\mathrm{eff}} = 8.739$, while from the 2-D and analytical formula, we obtain $Z_0^{2\mathrm{D}} = 10.21$, $\epsilon_{r\mathrm{eff}}^{2\mathrm{D}} = 8.12$, $Z_0^{a} = 9.88$, and $\epsilon_{r\mathrm{eff}}^{a} = 8.68$. In both of the above two examples the dynamic solution predicts identical results.

B. Evaluation of Discontinuity Parameters

We consider two striplines of widths $W_1 = 0.005\lambda_0$ and $W_2 = 0.05\lambda_0$ situated above a dielectric of $\epsilon_r = 10.0$ and $h = 0.01\lambda_0$. The line is treated as two strips. The currents at the discontinuity are not modeled very accurately as the structure is electrically small. From the $[Z]$ parameters, the S parameters are computed as

$$[S] = \left[(z+I)^{-1}\right][z-I]$$

where

$$z_{11} = \frac{Z_{11}}{Z_{01}} \qquad z_{12} = \frac{Z_{12}}{\sqrt{Z_{01}Z_{02}}}$$

$$z_{21} = \frac{Z_{21}}{\sqrt{Z_{01}Z_{02}}} \qquad z_{22} = \frac{Z_{22}}{Z_{02}}$$

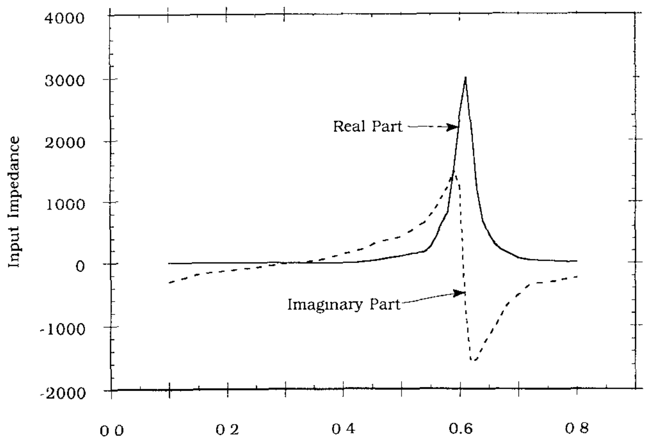

Fig. 9. The real and imaginary parts of the input impedance of a strip dipole antenna versus the normalized wavelength in terms of the free-space wavelength λ_0. The width of the strip is $0.01\lambda_0$, the dielectric height is $0.0796\lambda_0$, and the dielectric constant ϵ_r is 2.25.

where Z_{01} and Z_{02} are the characteristic impedances of lines 1 and 2. From the $[S]$ matrix, the discontinuity parameters are obtained by shifting the reference planes of both ports a distance 1 towards the discontinuity. Hence $[S_d] = [D][S][D]$, where

$$[D] = \begin{bmatrix} \exp(j\beta l) & 0 \\ 0 & \exp(j\beta l) \end{bmatrix}.$$

The β_i's and Z_{0i}'s are calculated utilizing the 3-D analysis. The $[S$ (magnitude, phase)$]$ matrix is computed as

$$[S] = \begin{bmatrix} (0.675, 8.39^\circ) & (0.7467, -12.4^\circ) \\ (0.7283, -1.13^\circ) & (0.675, -190.86^\circ) \end{bmatrix}.$$

The $[S]$ matrix is complex, and the phase is very small. We then do an approximate analysis by calculating the characteristic impedance of both lines utilizing a 2-D analysis and then we obtain the equivalent results by treating it as a simple junction of two lines with different characteristic impedances. This results in a real set of S parameters given by

$$[S] = \begin{bmatrix} 0.660 & 0.7505 \\ 0.7507 & -0.660 \end{bmatrix}.$$

Observe that the $[S]$ matrix is not symmetric. This is due to numerical errors incurred in the evaluation of the *ABCD* matrix. Hence the extracted Z or S parameters are not symmetric.

C. Computation of the Input Impedance of a Strip Antenna

The input impedance versus the normalized antenna length for a center-fed antenna is considered in this section. The strip is of width $W = 0.001\lambda_0$ situated over a dielectric of height $h = 0.0796\lambda_0$ (or $0.1186\lambda_{\mathrm{eff}}$) and $\epsilon_r = 3.25$. The real and imaginary parts of the input impedance are plotted in Fig. 9. They are similar to those predicted by a full-wave analysis in [8].

D. Evaluation of the Frequency-Dependent [S] Parameters of a Step Discontinuity

Consider a junction of line widths 1 mm and 0.25 mm situated at a height of 0.25 mm over a dielectric substrate of $\epsilon_r = 10.0$. The $[S]$ parameters are computed as functions of frequencies. The magnitude and phase at 12 and at 30 GHz obtained are given by

$$[S_{12}] = \begin{bmatrix} (0.412, -7.45°) & (0.9054, -0.626°) \\ (0.9176, -0.6674°) & (0.412, 6.239°) \end{bmatrix}$$

$$[S_{30}] = \begin{bmatrix} (0.4144, -9.84°) & (0.8938, -1.343°) \\ (0.9293, -1.63°) & (0.4154, 7.395°) \end{bmatrix}.$$

The results are then compared with [10] and reasonable agreement is found. Observe again that the S matrix is not symmetric.

VII. Conclusion

A quasi-dynamic solution, which incorporates the phase term over the quasi-static solution technique, for analyzing arbitrarily oriented microstrip lines has been presented. The region of validity of the quasi-dynamic solution has been investigated and is found to be much larger than the region of validity of the quasi-static solution. Finally numerical examples were presented to validate the new approach.

References

[1] J. R. Mosig and F. E. Gardiol, "Analytical and numerical techniques in the Green's function treatment of microstrip antennas and scatterers," *Proc. Inst. Elec. Eng.*, pt H, vol. 130, pp. 175–182, Mar. 1983.

[2] J. R. Mosig and T. K. Sarkar, "Comparison of quasi-static and exact electromagnetic fields from a horizontal electric dipole above a lossy dielectric backed by an imperfect ground plane," *IEEE Trans. Microwave Theory Tech.*, vol. MTT-34, pp. 379–387, Apr. 1986.

[3] C. M. Bulter, "The equivalent radius of a narrow conducting strip," *IEEE Trans. Antennas Propagat.*, vol. AP-30, pp. 755–758, July 1982.

[4] M. Kobayashi, "Longitudinal and transverse current distributions on microstrip lines and their closed-form expressions," *IEEE Trans. Microwave Theory Tech.*, vol. MTT-33, pp. 784–788, Sept. 1985.

[5] J. N. Venkataraman, S. M. Rao, A. R. Djordjevic, T. K. Sarkar, and Y. Naiheng, "Analysis of arbitrarily oriented microstrip transmission lines in multilayered dielectric media," *IEEE Trans. Microwave Theory Tech.*, vol. MTT-32, pp. 952–959, Oct. 1985.

[6] Y. L. Chow and I. El-Behery, "An approximate dynamic spatial Green's function for microstrip lines," *IEEE Trans. Microwave Theory Tech.*, vol. MTT-26, pp. 978–983, 1978.

[7] E. Rana and N. G. Alexopoulos, "Current distribution and input impedance of printed circuit," *IEEE Trans. Antennas Propagat.*, vol. AP-29, pp. 99–105, Jan. 1981.

[8] M. Marin, S. Barkeshli, and P. H. Pathak, "Efficient analysis of planar microstrip geometries using a closed-form asymptotic representation of the grounded dielectric slab Green's function," *IEEE Trans. Microwave Theory Tech.*, vol. 37, pp. 669–679, Apr. 1989.

[9] C. W. Davidson *Transmission Lines for Communications.* New York: Macmillan 1978.

[10] Z. Chen and B. Gao, "Deterministic approach to full-wave analysis of discontinuities in MIC's using the method of lines," *IEEE Trans. Microwave Theory Tech.*, vol. 37, pp. 606–611, Mar. 1989.

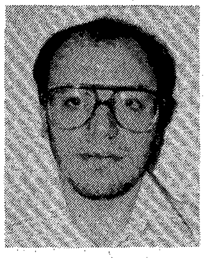

Tawfik Rahal Arabi (M'90) was born in Beirut, Lebanon, on December 3, 1964. He received the B.E.E. degree from the American University of Beirut, Beirut, Lebanon, in June 1985 and the M.S. degree from Syracuse University Syracuse, NY, in August 1987. Currently he is working toward the Ph.D. degree in the Department of Electrical Engineering at Syracuse University. His research interests are numerical problems in electromagnetics, especially those in the electronic packaging area.

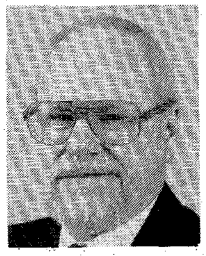

Arthur T. Murphy (S'49–A'54–M'54–SM'61–F'90) received the Ph.D. and M.S. degrees in electrical engineering from Carnegie-Mellon University and the B.E.E. degree from Syracuse University, Syracuse, NY.

He leads an Electronic Systems Research Group which guides R&D programs by evaluating end-use performance of DuPont Electronics products. He has an expertise in applications in high-speed electronic interconnections and electromagnetic interference. He has established a state-of-the-art laboratory and a unique computer-aided design system, called ICONSIMsm, for interconnection simulation. This has been used in designing advanced interconnection assemblies, rigid and flexible printed wiring boards, and ceramic and polymeric packages. He also recently developed a unique UHF filter which eliminates electromagnetic emission from computers. Before joining DuPont ten years ago, he was Brown Professor and Head of the Department of Mechanical Engineering at Carnegie-Mellon University and previously held positions of Vice President and Dean of Engineering at Widener University, Head of the Department of Electrical Engineering at Wichita State University, Visiting Professor at M.I.T. and at University of Manchester (England), and Adjunct Lecturer at Penn State University.

Tapan K. Sarkar (S'69–M'76–SM'81) was born in Calcutta, India, on August 2, 1948. He received the B. Tech. degree from the Indian Institute of Technology, Kharagpur, India, in 1969, the M.Sc.E. degree from the University of New Brunswick, Fredericton, Canada, in 1971, and the M.S. and Ph.D. degrees from Syracuse University, Syracuse, NY, in 1975.

From 1975 to 1976 he was with the TACO Division of General Instruments Corporation. He was with the Rochester Institute of Technology, Rochester, NY, from 1976 to 1985. He was a Research Fellow at the Gordon Mckay Laboratory, Harvard University, Cambridge, MA, from 1977 to 1978. He is now a Professor in the Department of Electrical and Computer Engineering at Syracuse University. His current research interests deal with the numerical solution of operator equations arising in electromagnetics and signal processing with application to system design. He has authored or coauthored over 154 journal articles and conference papers and has written chapters in eight books.

Dr. Sarkar is a registered professional engineer in the state of New York. He received the Best Paper Award of the IEEE TRANSACTIONS ON ELECTROMAGNETIC COMPATIBILITY in 1979. He also received one of the "best solution" awards in May 1977 at the Rome Air Development Center (RADC) Spectral Estimation Workshop. He was an Associate Editor for feature articles of the *IEEE Antennas and Propagation Society Newsletter* and the IEEE TRANSACTIONS ON ELECTROMAGNETIC COMPATIBILITY. He was the Technical Program Chairman for the 1988 IEEE Antennas and Propagation Society International Symposium and URSI Radio Science Meeting. Dr. Sarkar is an Associate Editor for the *Journal of Electromagnetic Waves and Applications* and is on the editorial board of the *International Journal of Microwave and Millimeter-Wave Computer Aided Engineering*. He has been appointed U.S. Research Council Representative to many URSI General Assemblies. He is also Chairman of the Intercommission Working Group of International URSI on Time Domain Metrology. He is a member of Sigma Xi and the International Union of Radio Science Commissions A and B.

Roger F. Harrington (S'48–A'53–M'57–SM'62–F'68) was born in Buffalo, NY, on December 24, 1925. He received the B.E.E. and M.E.E. degrees from Syracuse University, Syracuse, NY, in 1948 and 1950, respectively, and the Ph.D. degree from Ohio State University, Columbus, in 1952.

From 1945 to 1946, he served as an Instructor at the U.S. Naval Radio Materiel School, Dearborn, MI, and from 1948 to 1950 he was employed as an Instructor and Research Assistant at Syracuse University. While studying at Ohio State University, he served as a Research Fellow in the Antenna Laboratory. Since 1952, he has been on the faculty of Syracuse University, where he is presently Professor of Electrical Engineering. During the years 1959–1960, he was visiting Associate Professor at the University of Illinois, Urbana; in 1964 he was Visiting Professor at the University of California, Berkeley; and in 1969 he was Guest Professor at the Technical University of Denmark, Lyngby, Denmark.

Dr. Harrington is a member of Tau Beta Pi, Sigma Xi, and the American Association of University Professors.

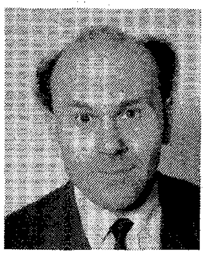

Antonije R. Djordjević was born in Belgrade, Yugoslavia, in 1952. He received the B.Sc., M.Sc., and D.Sc. degrees from the University of Belgrade in 1975, 1977, and 1979, respectively.

In 1975 he joined the Department of Electrical Engineering, University of Belgrade, where at present he is an Associate Professor of Microwaves. From February 1983 until February 1984 he was with the Department of Electrical Engineering, Rochester Institute of Technology, Rochester, NY, as a Visiting Associate Professor. His research focuses on numerical problems in electromagnetics, especially those applied to antennas and microwave passive components. He is a coauthor of a monograph on wire antennas and of two textbooks.